Contract No:

This document was prepared in conjunction with work accomplished under Contract No. 89303321CEM000080 with the U.S. Department of Energy (DOE) Office of Environmental Management (EM).

Disclaimer:

Removal of CrO_4^{2-}, a Nonradioactive Surrogate of $^{99}TcO_4^-$, Using LDH─Mo_3S_{13} Nanosheets

Ahmet Celik[a], Dien Li,[b] Michael Quintero,[c] Kathryn Taylor-Pashow[b], Xianchun Zhu,[d] Mohsen Shakouri,[e] Subrata Chandra Roy,[a] Mercouri G. Kanatzidis[c], Zikri Arslan,[a] Alicia Blanton,[a] Jing Nie,[a] Shulan Ma,[f] Fengxiang X. Han,[a] Saiful M. Islam[a]*

[a]*Department of Chemistry, Physics, and Atmospheric Sciences, Jackson State University, Jackson, MS, 39217, USA*
[b]*Savannah River National Laboratory, Aiken, SC, 29808, USA*
[c]*Department of Chemistry, Northwestern University, Evanston, IL, 60208, USA*
[d]*Department of Civil Engineering, Jackson State University, Jackson, MS, 39217, USA*
[e]*Canadian Light Source, Saskatoon, SK, S7N 0X4, Canada*
[f]*College of Chemistry, Beijing Normal University, Beijing 100875, China*

ABSTRACT: Removal of chromate (CrO_4^{2-}) and pertechnetate (TcO_4^-) from the Hanford Low Activity Waste (LAW) is beneficial as it impacts the cost, life cycle, operational complexity of the Waste Treatment and Immobilization Plant (WTP), and integrity of vitrified glass for nuclear waste disposal. Here, we report the application of $[Mo^{IV}{}_3S_{13}]^{2-}$ intercalated layer double hydroxides (LDH─Mo_3S_{13}) for the removal of CrO_4^{2-} as a surrogate for TcO_4^-, from ppm to ppb levels from water and a simulated LAW off-gas condensate of Hanford's WTP. LDH─Mo_3S_{13} removes CrO_4^{2-} from the LAW condensate stream, having a pH of 7.5, from ppm (~ 9.086 ×10^4 ppb of Cr^{6+}) to below 1 ppb levels with distribution constant (K_d) values of up to ~10^7 mL/g. Analysis of post-adsorbed solids indicates that CrO_4^{2-} removal mainly proceeds by reduction of Cr^{6+} to Cr^{3+}. This study sets the first example of a metal-sulfide intercalated LDH for the removal of CrO_4^{2-}, as relevant to TcO_4^-, from the simulated off-gas condensate streams of Hanford's LAW Melter which contains highly concentrated competitive anions, namely F^-, Cl^-, CO_3^{2-}, NO_3^-, BO_3^{3-}, NO_2^-, SO_4^{2-}, and $B_4O_7^{2-}$. LDH─Mo_3S_{13}'s remarkable removal efficiency

make it a promising sorbent to remediate CrO_4^{2-}/TcO_4^- from surface water and off-gas condensate of nuclear waste.

Keywords: nuclear waste, pertechnetate, chromate, low activity waste, off-gas condensate stream, Hanford's radioactive waste

Synopsis: This study introduces LDH─Mo_3S_{13} nanosheets as a highly efficient multi-mode sorbent of CrO_4^{2-}/TcO_4^- from the high ionic strength off-gas condensate streams generated from processing defense legacy LAW.

TOC:

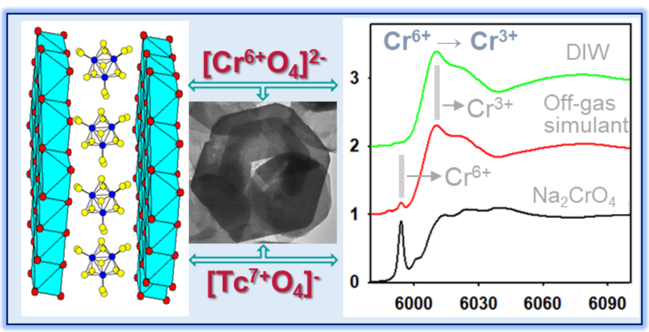

INTRODUCTION

The Hanford Waste Treatment and Immobilization Plant (WTP), the DOE's largest nuclear waste treatment plant, is designed to process, treat, and immobilize much of the radioactive legacy wastes.[1–4] The current plan of the Hanford Waste Treatment and Immobilization Plant (WTP) is to separate the tank wastes into high-level waste (HLW) and low-activity waste (LAW) and permanently immobilize the radioisotopes into separately vitrified waste forms.[5] LAW constitutes a larger fraction of the waste by volume and it consists of high ionic-strength solutions that contain Na^+, K^+, $Al(OH)_4^-$, Cl^-, F^-, NO_2^-, NO_3^-, OH^-, CO_3^{2-}, organics, and other minor ions of Cr, Ni, Cd, Pb, and radionuclides.[6] Technetium-99 (^{99}Tc) is a β-emitting long living, $t_{1/2}$ ~ 2.13×10^5 years, radionuclide which mostly remains in LAW as TcO_4^-.[4,7–10] Immobilization of TcO_4^- at the WTP becomes challenging because of its high solubility, complex redox chemistry, and volatility at the vitrification temperature.[4,7–10] The treatment and vitrification of LAW at the Hanford WTP will generate an aqueous LAW off-gas condensate which is planned to be repeatedly reprocessed and passed through the glass melter until nearly complete immobilization of technetium.[4,8,11] This procedure result in the increase of the WTP operational time, waste volume and vitrification cost. Importantly, this process could be limited for extremely low concentrations, namely ≤ 5 ppb. Also, the off-gas condensate contains halides and chromates which have detrimental effect on the glass formulation during the vitrication.[12–14] Therefore, it is important to develop materials, methods, and technologies to redirect the technetium immobilization from LAW.

With a reduction potential of -0.22 V (for the S^{2-}/SO_4^{2-} couple), sulfides are capable of reducing the highly soluble TcO_4^- (TcO_4^-/Tc^{4+} is E^o ~ +0.74 V) and CrO_4^{2-} (CrO_4^{2-}/Cr^{3+} is E^o ~ +1.23 V) ions to insoluble Tc(IV) and Cr(III) species.[6,15–21] Because of the known chemistry of sulfides and other reductants for the reductive precipitation of highly redox-active Tc^{7+} and Cr^{6+}, we introduced $(Cr^{6+}O_4)^{2-}$ as non-radioactive surrogate for a reductive precipitation driven separation.[1,9,22,23] In addition to being a suitable surrogate for TcO_4^-, CrO_4^{2-} itself is highly toxic[24] and also persists within the radioactive waste of the Hanford nuclear waste streams.[25–27] Because of the leakage in the Hanford underground tanks, chromate has been dispersing in the environment along with various radionuclides.[28–30] Moreover, during the vitrification process of the LAW, CrO_4^{2-} is transformed into crystalline spinel which in turn jeopardizes the integrity of the glass waste form.[13,31] Therefore, in addition to pertechnetate it is crucial to remediate chromate from water and legacy nuclear wastes.

Numerous metal sulfides, such as pyrrhotite ($Fe_{1-x}S$) and pyrite (FeS_2),[32,33] chalcocite (Cu_2S),[29,30] stibnite (Sb_2S_3),[34] and layered metal-sulfides[6] are known to immobilize TcO_4^- by reductive precipitation.[15,16] Layered double hydroxides (LDHs) are anionic clays which can also remove TcO_4^-/CrO_4^{2-} but with ion-exchange and surface sorption mechanisms.[8,15,24,35] Considering the efficiency of LDH and metal-sulfides for TcO_4^-/CrO_4^{2-} remediation, we hypothesized that a hybrid structure of metal-sulfide intercalated LDH will boost the removal of pertechnetate from water and legacy nuclear waste. Altogether, it becomes important to investigate LDH-metal-sulfide based materials, evaluate the remediation of TcO_4^- and delineate the sorption mechanisms involved in this process.

Herein, we report a modified synthesis method for LDH─Mo_3S_{13}[36] to achieve nanosheets and the investigation of CrO_4^{2-}, which also acts as a TcO_4^- surrogate, sorption from naturally contaminated surface water and simulated off-gas condensate of the LAW melter. We show that LDH─Mo_3S_{13} exhibits ultrahigh efficient sorption of CrO_4^{2-} from water and off-gas condensate from ppm to ppb levels (<1 ppb) with K_d values of up to ~10^7 mL/g. For LDH─Mo_3S_{13}, we show that reductive precipitation is the dominant mechanism, however, ion-exchange and/or surface sorption can provide parallel paths for the sequestration of CrO_4^{2-}. These integrated multimode sorption processes make LDH─Mo_3S_{13} a promising sorbent of CrO_4^{2-} / TcO_4^- from polluted water and nuclear waste.

EXPERIMENTAL

Material synthesis and chromate uptake study: MgAl─CO_3 (LDH─CO_3), MgAl─NO_3 (LDH─NO_3) and $(NH_4)_2Mo_3S_{13}\cdot H_2O$ were synthesized as previously described.[37,38,39,40] LDH─Mo_3S_{13} nanosheets were synthesized with a two-step method. First, exfoliation of LDH nanosheets of the LDH─NO_3 and then the settlement of positively charged LDH sheets in the presence of dissolved $Mo_3S_{13}^{2-}$ anions. More specifically, 200 mg LDH─NO_3 was added to 20 mL formamide and was stirred for 24 h to exfoliate the positively charged LDH nanosheets. Afterward, a solution of 200 mg of $(NH_4)_2Mo_3S_{13}\cdot H_2O$ in 2 mL formamide was slowly added to the exfoliated LDH solution and stirred for 30 minutes. Later, the solution was left at ambient conditions for 2 h, filtered, and then washed with water, acetone and subsequently dried at ambient conditions to give a brown solid of LDH─Mo_3S_{13}. Thus, this process of synthesis differs from the previously reported synthesis of LDH─Mo_3S_{13}.[36]

Chromate uptake study: LDH─Mo_3S_{13} was added to the CrO_4^{2-} spiked solutions at different concentrations, stirred for different periods of time, and centrifuged to separate the supernatant solution from the solids. For the Hanford's LAW off-gas condensate simulated streams,[1] the sorption study was conducted by the batch method by spiking the simulant with 9.086×10^4 ppb of Cr^{6+} as CrO_4^{2-} (CrO_4^{2-} equivalent concentrations ~2.027×10^5 ppb); using variable loading of adsorbent, LDH─Mo_3S_{13} (10 to 100 mg) and at variable time scales (~1 h to 7 d), in 10 mL of simulated solutions, as described in Table S1.[1,9] This study mostly focuses on the application of the LDH material for the remediation of CrO_4^{2-}/TcO_4^- from the high ionic strength simulated off-gas condensate streams of Hanford LAW waste at pH ~7.5. Hence the variation of the solution pH and ionic strengths were not monitored or controlled during the Cr uptake studies since these are not known for the real off-gas condensate streams as the WPT has not started this operation yet.

After the sorption experiments, the residual CrO_4^{2-} concentrations in the supernatant were analyzed by inductively coupled plasma-mass spectrometry (ICP-MS). The adsorption capacity was determined from the difference in the concentrations of Cr before and after sorption.

The distribution coefficient (K_d) for the sorption of CrO_4^{2-} was determined in accordance with the equations, $K_d = (V[(C_0 - C_f)/C_f])/m$; where V is the solution volume (mL), C_0 and C_f are the initial and the final concentrations of CrO_4^{2-} in ppm, and m is the mass of the solid sorbent (g).[41] In this work, we used the K_d values to compare the Cr^{6+} removal performance with other adsorbents. The removal rate of CrO_4^{2-} was computed using the equation of $100\times(C_0 - C_f)/C_0$. The removal capacity, q_m (mg/g) can be obtained from the equation: $10^{-3} \times (C_0 - C_f)V/m$. The adsorption experiments were carried out with V:m ratios of 100-1000 mL/g, at room temperature (RT) and at different time scales ranging from minutes to days.

The sorption kinetics of LDH─Mo_3S_{13} was studied to determine the rate of removal of CrO_4^{2-} and to understand the sorption mechanism. In general, the adsorption rate is determined by two different rate equations, known as pseudo-first order, and pseudo-second-order mechanisms. Here, we used these mechanisms to analyze the adsorption phenomena of LDH─Mo_3S_{13}. The comparison was then drawn between the experimental and calculated data in accordance with the rate equations, as follows.[42]

Pseudo-first-order:

$$\ln(q_e - q_t) = \ln q_e - k_1 t \qquad (1)$$

Pseudo-second-order:

$$\frac{t}{q_t} = \frac{1}{k_2 q_e^2} + \frac{t}{q_e} \qquad (2)$$

Where, q_e (mg/g) is the amount of adsorbed element per unit mass of adsorbent at equilibrium and q_t (mg/g) is the adsorbed amount at time t, while k_1 (min^{-1}) and k_2 ($g/mg \cdot min^{-1}$) are equilibrium rate constants of pseudo-first-order and pseudo-second-order adsorption interactions, respectively.[43] The k_1 value can be obtained by plotting $\ln(q_e\text{-}q_t)$ against t and k_2 by plotting t/q_t against t.

To understand the adsorbent and adsorbate interactions, we demonstrate the experimentally obtained adsorption data using the Langmuir isotherms model as given in equation 3. According to this model, the adsorbate moieties undergo monolayer type coverage on the surface of the adsorbent materials. It also predicts, once an adsorption site is occupied, no further adsorption can occur at the same site.[44] The Langmuir isotherm model for heterogenous models is shown as equation (3):

$$\text{Langmuir isotherm: } q = q_m \frac{bC_e}{1+bC_e} \qquad (3)$$

where C_e (mg/L) is the concentration at equilibrium, q (mg/g) is the equilibrium sorption capacity of the adsorbed CrO_4^{2-}, q_m (mg/g) is the theoretical maximum sorption capacity, b ($L \cdot mg^{-1}$) is the Langmuir constant which is related to the interaction energy of LDH─Mo_3S_{13} and CrO_4^{2-}.

Characterization: Samples were analyzed by scanning electron microscopy (SEM), transmission electron microscopy (TEM) and Energy Dispersive Spectroscopy (EDS), X-ray Powder Diffraction (XRD) and Infrared (FT-IR) Spectroscopy, and Inductively Coupled Plasma-

Mass Spectrometry (ICP-MS), and X-ray photoelectron spectroscopy (XPS) (see supporting information file for experimental details).

Synchrotron X-ray Absorption Spectroscopy: The solid samples after the chromate interactions in DIW and simulated solutions were dried at ambient conditions and analyzed by synchrotron X-ray absorption near edge structure (XANES) and extended X-ray absorption fine structure (EXAFS*)*. S K-edge and Mo L_3-edge XANES and Cr K-edge EXAFS measurements were performed at the Soft X-ray Microcharacterization Beamline (SXRMB) of the Canadian Light Source (CLS), Saskatoon, Canada. SXRMB is a bending-magnet-based beamline that utilizes InSb(111) and Si(111) crystals for monochromatization to cover an energy range of 1.7–10 keV. Samples were mounted onto double-sided, conductive carbon tape and loaded into the vacuum chamber with vacuum of 10^{-7} torr. Na_2CrO_4 and $HgSO_4$ were used as references and for energy calibration. A 7-element SDD detector was used to record the fluorescence yield (FY) of the powder samples. The total electron yields (TEY) by recording the drain current off the sample was also recorded. The collected data were processed and analyzed using the Demeter software package including Athena and Artemis.[45] Data from multiple scans were processed using Athena by aligning and merging the spectra followed by background subtraction using the AUTOBK algorithm. Chromium K-edge EXAFS data analysis was conducted on the merged and normalized spectra using Artemis. Theoretical models were constructed with the program FEFF7. Cr_2O_3 was used as a reference structural model.[46] Fits to the Cr EXAFS data were made in R space (R from 1 to 3.2 Å) and obtained by taking the Fourier Transform (FT) of $\chi(k)$ (k from 1.5 to 10.5) with a k weighting of 3.

RESULTS AND DISCUSSION

Synthesis and characterization of LDH─Mo_3S_{13} nanosheets: The LDH─Mo_3S_{13} hybrid nanosheets were synthesized using a novel two step method starting from LDH─NO_3 that involves (i) the chemical exfoliation of LDH─NO_3 and (ii) the subsequent treatment of the exfoliated ultra-thin LDH nanosheets by $[Mo_3S_{13}]^{2-}$ anion (Figure 1). This modified synthesis is advantageous over the previously reported method[36] because it reduces ~ 90% of the organic solvents and time to produce LDH─Mo_3S_{13}. A shorter interaction time in the solution can help to produce LDH nanosheets, retain the integrity of $[Mo_3S_{13}]^{2-}$ anions, and avoid the side reactions. SEM and TEM images reveal the platelike morphology of LDH─Mo_3S_{13} nanosheets (Figures 1A and 1B). EDS determines the average abundance of Mg, Al, Mo, and S are 20.8, 13.4, 12.4, and 53.4 in atomic percentage, respectively. Here, the Mo:S ratio is ~ 1:4.3 which is aligned to the composition of $[Mo_3S_{13}]^{2-}$ anions. Elemental mapping of SEM micrographs further confirms the uniform distributions of Mg, Al, Mo, and S across the LDH─Mo_3S_{13} crystallites (Figure S1). Infrared spectrum of the LDH─NO_3 shows a very strong peak at about 1370 cm^{-1} that corresponds to the stretching vibration of NO_3^- anions,[47,48] while for LDH─Mo_3S_{13} the intensity of the 1370 cm^{-1} peak is markedly diminished (Figure 1C). This demonstrates the exchange of NO_3^- with $[Mo_3S_{13}]^{2-}$ anions between the positively charge nanosheets of LDH.

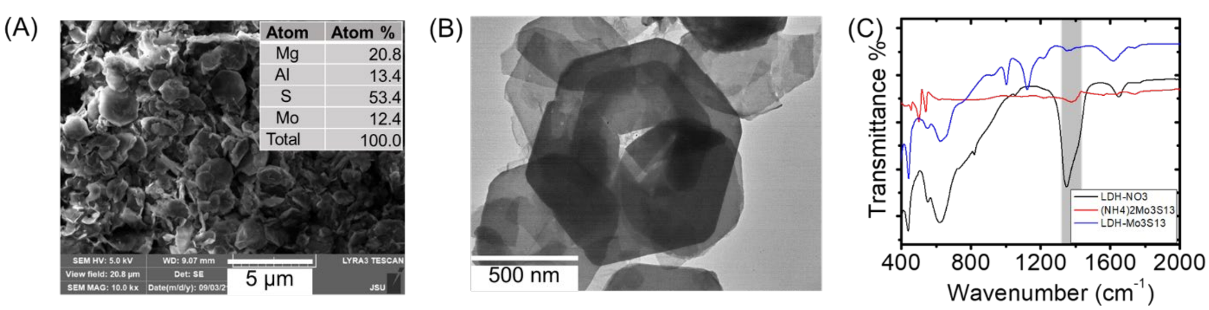

Figure 1: SEM image of the as-prepared LDH─Mo_3S_{13}, insets show the average atomic abundance in percentage that was obtained by EDS (A), TEM image showing the ultrathin

platelike morphology of the crystallites (B), infrared spectrum showing the absence of NO_3^- peaks from the LDH─Mo_3S_{13} indicating ion exchange of nitrate by the Mo_3S_{13} (C).

Sorption of CrO_4^{2-} from water: The sorption experiments with Cr^{6+} show that LDH─Mo_3S_{13} nanosheets are highly efficient for the sequestration of CrO_4^{2-} from water under acidic, neutral, and alkaline conditions (Table S2). At neutral pH, from a 1000 ppb of Cr^{6+} (CrO_4^{2-}) spiked deionized water (DIW) solution, LDH─Mo_3S_{13} can capture over 99.99% of Cr^{6+} leaving the final concentration below 1 ppb with K_d value of ~ 1.0×10^7 mL/g in 24 h (Tables S2 and S3). This concentration is well below the tolerance limits provided by the U.S. EPA (100 ppb) and WHO (50 ppb) for drinking water.[49,50] Also, it should be noted that the value of K_d is higher to or comparable to other high performing materials known in literature.[18,24] At pH~11, LDH─Mo_3S_{13} can sequester over 98.7% of Cr^{6+} decreasing the final concentration to 13 ppb with the K_d ~ 7.7×10^4 mL/g in 48 h. Conversely, at pH ~ 2, LDH─Mo_3S_{13} can sequester over 74% of Cr^{6+} ions. The lower effectiveness at this pH may be attributed to the slow decomposition of LDH─Mo_3S_{13}. A similar experiment with 10-fold higher Cr^{6+} concentration revealed similar adsorption efficiencies of over 79.2, 99.9 and 91.9% at pH ~2, 7 and 11, respectively (Table S2). Noticeably, despite the 10-fold increase of Cr^{6+} concentrations in the solutions, the residual concentrations, especially at neutral pH, remains below 10 ppb with K_d values of $\geq 10^6$ mL/g. Overall, our experiments show that LDH─Mo_3S_{13} is highly efficient to remove Cr^{6+} from neutral and alkaline media.

The kinetic study of LDH─Mo_3S_{13} for the removal of Cr^{6+} was conducted using initial concentrations of 1.0×10^3 and 1.0×10^4 ppb of Cr^{6+} in DIW (Figures 2A and 2B, Tables S3 and S4). The experimental data were fitted with the pseudo-second order rate equation that yielded the coefficient of determination, $R^2 > 0.99$ (Figure 2C, Table S5). The pseudo-second-order rate constants were determined to be 0.0886±0.0572 and 0.0015±0.0003 g/mg·min^{-1} for 1.0×10^3 and 1.0×10^4 ppb of Cr^{6+} solutions, respectively. The difference in rate constants is indicative of different sorption mechanisms at different initial concentrations. Apart from this, the higher rate constant indicates faster sorption kinetics of Cr^{6+} for the 1.0×10^3 ppb solution.

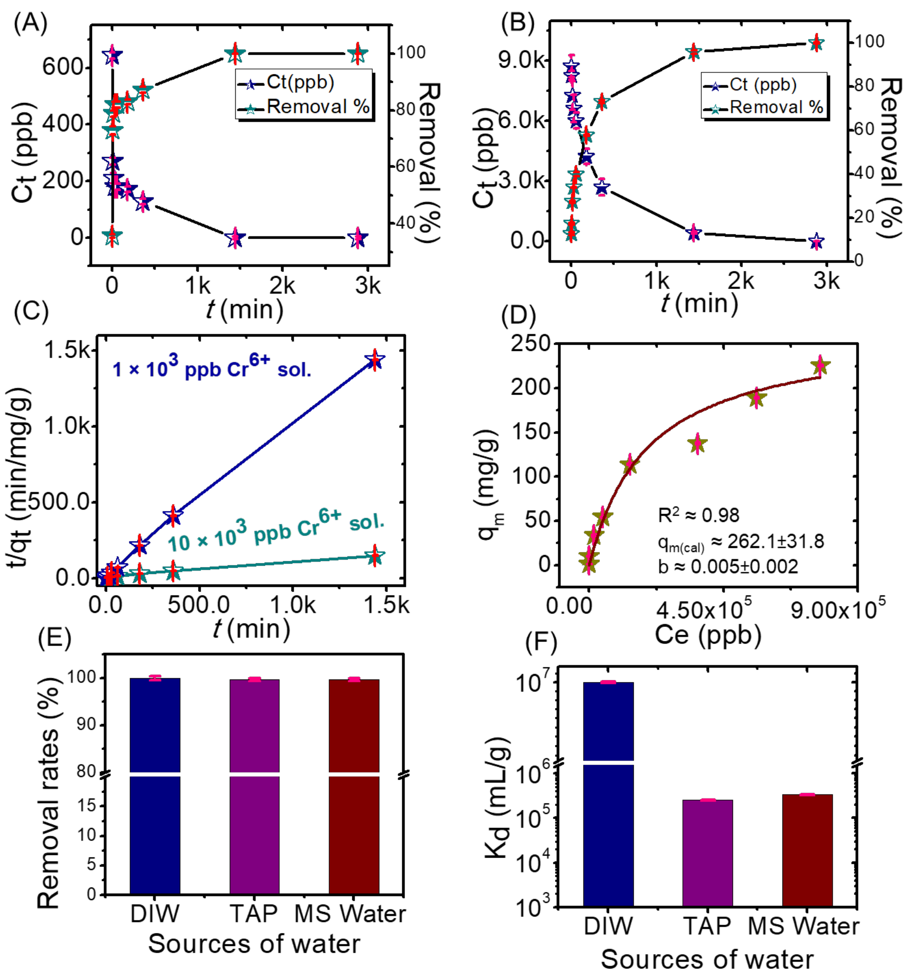

Figure 2: Adsorption kinetics for the residual concentrations (C_t) and removal rates of Cr^{6+} for 1.0×10^3 ppb (A) and 1.0×10^4 ppb (B) solutions in DIW; a comparison of the pseudo second-order adsorption kinetics for 1×10^3 and 1×10^4 ppb solutions (C); adsorption capacity, q_m vs equilibrium adsorption concentrations, C_e (D); a comparable study of the sorption of Cr^{6+} from CrO_4^{2-} spiked DIW, Tap, and Mississippi River water showing the removal rate (E) and distribution coefficient (F). These experiments were conducted using 10 mg of LDH─Mo_3S_{13} in 10 mL (v/m ~1000 mL/g) of solutions at room temperature and pressure for a period of 48 h for (A - D) and 24 h for (E – F). The blue and blue-green stars in A-B represent C_t and removal percentage, respectively. In C the blue and blue-green stars represent 1.0×10^3 and 1.0×10^4 ppb of Cr^{6+} concentration; golden yellow stars in D represent equilibrium concentrations, the red bars in A-F represent standard deviations.

To evaluate Cr^{6+} uptake capacity and adsorption isotherm, we investigated the sorption of Cr^{6+} for a broad range of concentrations, 1.0×10^3 to 1.0×10^5 ppb (Figure 2D, Table S6). This study reveals that the sorption capacity increases with the increase of Cr^{6+} concentrations until it reaches an equilibrium. Our experiment determines that the maximum adsorption of Cr^{6+} is about 225 mg/g. This value of sorption capacity is superior to other high performing materials, namely LDH─MoS_4 ~ 130 mg/g and CoAl─LDH ~ 93.5 mg/g,[18,24] cationic aluminum oxyhydroxides ~105.4 mg/g,[51] anion exchange resin, (IRN78 ~63.5 mg/g),[51] and comparable to metal organic frameworks (MOR-1-HA ~242),[52] and non-LDH cationic layered material, (TJU-1 ~ 279 mg/g).[26] The experimentally obtained Cr^{6+} sorption isotherm data are fitted with the Langmuir model which yielded the R^2 ~ 0.98 (Figure 2D). The Langmuir constant, *b* was obtained as 0.005(2) L/mg and is comparable to other Cr^{6+} adsorbents.[53]

To determine the effectiveness of LDH─Mo_3S_{13} for Cr^{6+} removal in the presence of highly competitive ions in purified and naturally contaminated water, we investigated Cr^{6+} removal efficiency from tap water and Mississippi River water (collected from Vidalia, Louisiana) by spiking them with 1000 ppb of Cr^{6+} (CrO_4^{2-}) (Figures 2E and 2F; Table S7). This study showed that despite presence of numerous ions, such as Ca^{2+}, Mg^{2+}, Na^+, K^+, HCO_3^-, SO_4^{2-}, Cl^-, and other organic or inorganic constituents, LDH─Mo_3S_{13} can remove ≥99.6 % of Cr^{6+}. Such a high removal rate is indicative of the higher efficiency of LDH─Mo_3S_{13} for CrO_4^{2-} removal. Such an ultra-high removal decreased its final concentration to <5 ppb with $K_d \sim 10^5$ mL/g. These values are close to the values obtained for DIW as discussed above. This finding suggests that LDH─Mo_3S_{13} is effective at sequestration of Cr^{6+} even in the presence of highly competitive ions.

Removal of CrO_4^{2-}, a surrogate of TcO_4^-, from simulated off-gas condensate of Hanford's LAW: To evaluate the removal efficiency of LDH─Mo_3S_{13} for chromate, a non-radiogenic surrogate of $^{99}TcO_4^-$, we investigated simulated LAW Melter off-gas condensate of the Hanford's WTP (Figure 3; Tables S8-12). The simulant was prepared following a procedure described by Taylor-Pashow *et al.*[4,9] The chemical composition of the simulant consists of high concentrations of anions, e.g. F^-, Cl^-, CO_3^{2-}, NO_3^-, BO_3^{3-}, NO_2^-, SO_4^{2-}, and $B_4O_7^{2-}$ at pH ~7.5.

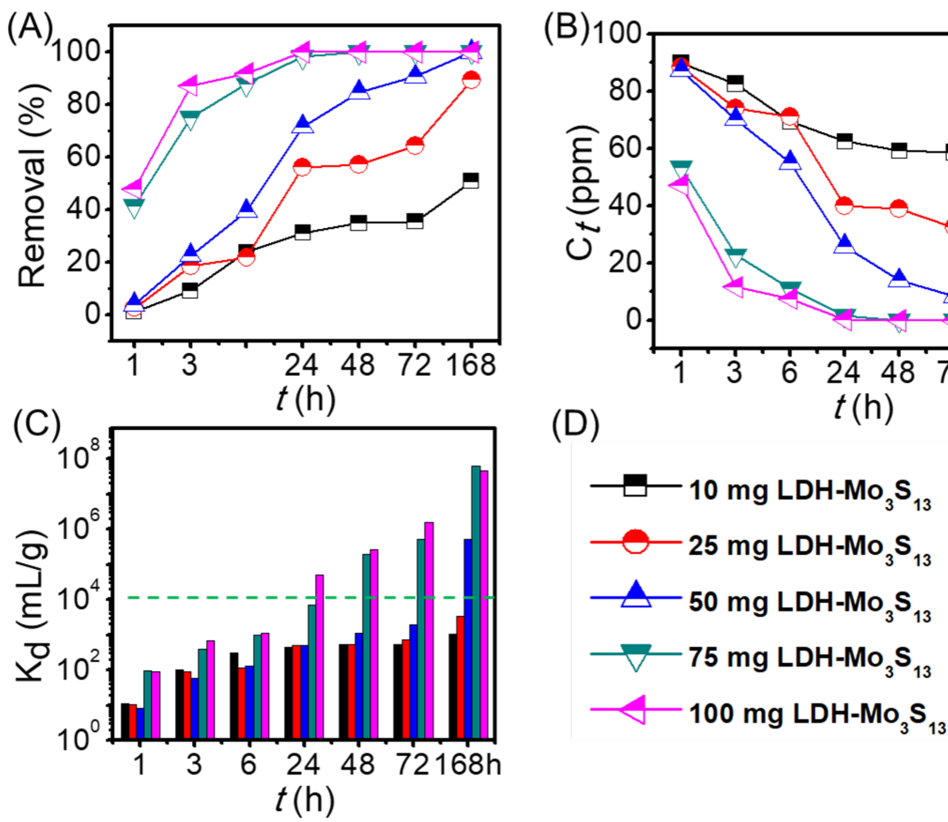

Figure 3: Time-dependent sorption of CrO_4^{2-} with an initial concentration of 9.086 ×10^4 ppb of Cr^{6+} as CrO_4^{2-} (CrO_4^{2-} equivalent concentrations ~2.027×10^5 ppb) as a non-radioactive surrogate of TcO_4^- from the simulated off-gas condensate of Hanford's LAW Melter with respect to various amounts of loading of the sorbents showing the removal (%) of CrO_4^{2-} (A), residual chromate concentration in the simulant (B), and the variation of K_d (mL/g) (C). Panel (D) represents the symbols that demonstrate the various amounts of LDH─Mo_3S_{13} used for this experiment. These experiments were conducted using 10 mg of LDH─Mo_3S_{13} in 10 mL (v/m ~1000 mL/g) of simulant solutions at room temperature and pressure for a period of 1 h through 68 h. Each experiment was replicated four times, and the average was considered to plot the diagram and analyze the results.

We observed that for the 10 and 25 mg loading of LDH─Mo_3S_{13}, the maximum removal of Cr^{6+} was about 50.7 and 89.3%, respectively from a 9.086×10^4 ppb Cr^{6+} spiked simulated solutions after seven days of interactions (Figures 3A and 3B, Tables S8-9). This value of removal rate and K_d is remarkably higher than that of the LDH─NO_3 and $(NH_4)_2Mo_3S_{13;}$ suggesting the importance of the LDH─Mo_3S_{13} for the ultra-high removal of Cr^{6+} ions from the simulated solution (Table S13). Conversely, for an interaction of 50 mg of LDH─Mo_3S_{13}, Cr^{6+} removal reached > 99.7% in 7 d. This leads to the residual concentration of Cr^{6+} to ~35 ppb and K_d values of ~5×10^5 mL/g (Figure 3C and Table S10). With a higher loading of 75 and 100 mg of LDH─Mo_3S_{13}, the removal of Cr^{6+} reached over 99.9 and 99.7 % only in 2 and 1 d, respectively (Figure 3C and Tables S11-12). Importantly, after 3 days the residual concentrations reach trace levels, 23 (75 mg) and 6 ppb (100 mg) and the K_d values reach $\geq 10^5$ mL/g. Besides, after 7 d of exposure, removal percentages reach ~100%; residual concentrations become as low as < 0.1 ppb, and the K_d reach ~10^7 mL/g. Herewith, LDH─Mo_3S_{13} demonstrates itself a highly efficient sorbent of CrO_4^{2-} and by extension also its TcO_4^- surrogate from the simulated off-gas condensate of the LAW Melter.

Understanding the adsorption mechanisms: The EDS and elemental mapping of the solid samples after the reaction with CrO_4^{2-} in DIW and simulated solution show the presence chromium across the sorbents (Figures S2 and S3). The SEM and TEM images of the solid sorbents after the adsorption study show the retention of the platelike morphology (Figures S2 and S3). The TEM of the post-interacted solids shows the presence of hexagonal crystallites similar to pristine LDH─Mo_3S_{13}. For the simulant treated samples the crystallites' surface becomes deteriorated which could be the impact of highly concentrated anions of F^-, Cl^-, and others.

XPS analysis of the pristine and loaded LDH─Mo_3S_{13} revealed the chemical state of the Mo, S and Cr ions (Figure 4, Table S14). The post treatment solid samples of LDH─Mo_3S_{13} shows the doublet of the peaks in the range of 570 – 595 eV corresponding to Cr 2p orbitals. As expected, these peaks are absent in the pristine LDH─Mo_3S_{13}. Specifically, the post adsorbed samples in water show the peaks at 586.2 eV/576.7 eV corresponding to the Cr^{3+} oxidations state, probably the formation of Cr_2O_3. Hence the doublet of peaks is the result of the spin-orbit splitting of the Cr^{3+} 2p orbitals.[18,54] For the samples that were treated with simulated solutions, the XPS show two pairs of peaks at 577.5 eV/585.5 eV and 589.1 eV/579.5 eV. The bands at 577.5 eV/585.5 eV can be originated from Cr^{3+} while the peaks at higher energy are attributed to Cr^{6+} ions of the CrO_4^{2-}.[54,55] The S 2p peaks that are observed in the range of 169.2─171.2 eV can be attributed to the oxidation of sulfides to sulfate anions (Figure S4).[56–58] Similarly, for the Mo 3d the weak peaks that are observed at about 236 eV are the results of the partial oxidation of Mo^{4+} to Mo^{6+} of the $Mo^{4+}{}_3S_{13}$ moieties of LDH─ Mo_3S_{13} (Figure S4).[59,60]

Furthermore, ICP analysis shows the presence of molybdenum ions in the post interaction solutions. A quantitative analysis by ICP MS determined that ~ 21% of Mo of LDH─Mo_3S_{13} dissolves. The presence of molybdenum ions can be attributed to oxidation dissolution of Mo^{4+} of the $[Mo^{4+}{}_3S_{13}]^{2-}$ to Mo^{6+} ions. The dissolution of Mo^{6+} results in the concurrent dissolution of sulfide which is likely to oxidize to sulfate/sulfite anions. Hence, this study reveals that a cooperative oxidation of both sulfur and molybdenum likely enhances the reduction of Cr^{6+} to Cr^{3+}.

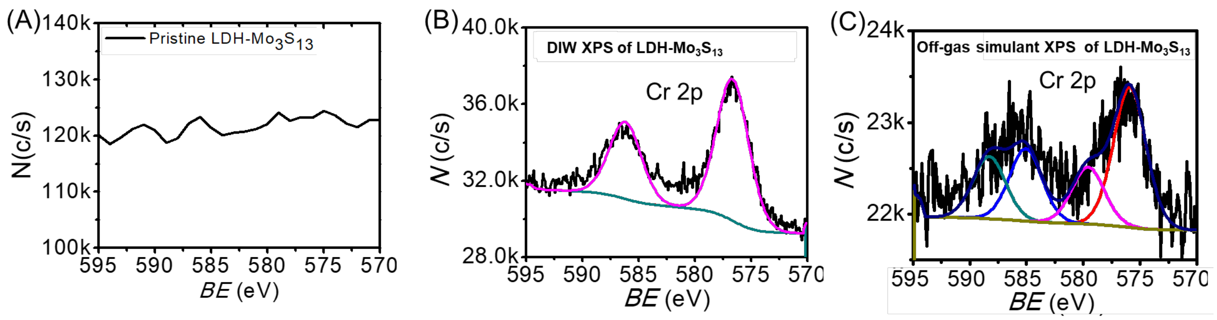

Figure 4: XPS spectra were collected for the pristine LDH─Mo_3S_{13} showing the absent of Cr (A), the DIW XPS data (B) and simulant XPS (B) show the presence of Cr. The DIW data was collected after the sorption experiments for 1×10^5 ppb of Cr^{6+} using 10 mg of LDH-Mo_3S_{13} in DIW, and the simulant XPS was collected for 9.086 $\times10^4$ ppb of Cr^{6+} treated solution after treating the solutions using 100 mg of LDH─Mo_3S_{13}. Each experiment was conducted 10 mL of solutions.

The Cr K-edge XANES spectra of LDH─Mo_3S_{13} samples were collected after reaction with CrO_4^{2-} in DIW and simulated LAW off-gas condensate, together with Na_2CrO_4 as a model compound (Figure 5A). For Na_2CrO_4, a sharp edge peak at 5994.0 eV is observed which is characteristic of the four coordinated character of the hexavalent chromate ion (CrO_4^{2-}).[61,62] Conversely, this peak at 5994.0 eV nearly completely disappeared for the DIW interacted sample, suggesting that Cr^{6+} was hardly detectable and the dominant species was Cr^{3+} reduced from CrO_4^{2-}. Additionally, there was another weak peak at 5991.2 eV, which is a typical pre-edge peak for Cr_2O_3 or $Cr(OH)_3$.[54,63] The solid sorbent obtained from the simulant experiment shows the presence of the peak at 5994.0 eV representative of CrO_4^{2-} ions. It is estimated from the Cr K-edge XANES there is ~15% CrO_4^{2-} and ~85% Cr^{3+} in this sample. In addition, there was a new peak at 5988.2 eV, together with a bump at 5991.2 eV corresponding to the pre-edge peak observed for the DIW treated sorbent. These two features are attributed to the split of the pre-edge and are assigned to Cr 1s transitions to 3d (t_{2g}) and 3d (e_g) electronic states, respectively, in the polyhedra of Cr^{3+} ions.[64] Overall, the Cr K-edge of XANES spectra of Na_2CrO_4 and post interacted LDH─Mo_3S_{13} in DIW and simulant illustrate features that are consistent with Cr valence state and change in coordination number. Notably, the reductive precipitation of $Cr^{6+} \rightarrow Cr^{3+}$ could be attributed to the presence of highly redox active sulfide anions in LDH─Mo_3S_{13}. Hence, a higher redox potentials of Tc^{7+} (TcO_4^-/Tc^{4+} is $E^o \sim +0.74$ V)[21] and Cr^{6+} (CrO_4^{2-}/Cr^{3+} is $E^o \sim +1.23$ V)[20] enable their reduction by the mono and disulfides species, $S^{2/1-} \rightarrow S^{n+} + ne^-$ (e.g. E^o of S^{2-}/SO_4^{2-} is ~ -0.22 V),[23] of LDH─Mo_3S_{13}. This reduction immobilizes Tc^{4+} /Cr^{3+} salts by the deposition of technetium and chromium containing solids on the sorbent. Since this reductive precipitation is the dominant mechanism for the sequestration of Cr^{6+}, and the sorbents is contaminated with the precipitated solids, this material is unlikely to be reusable.

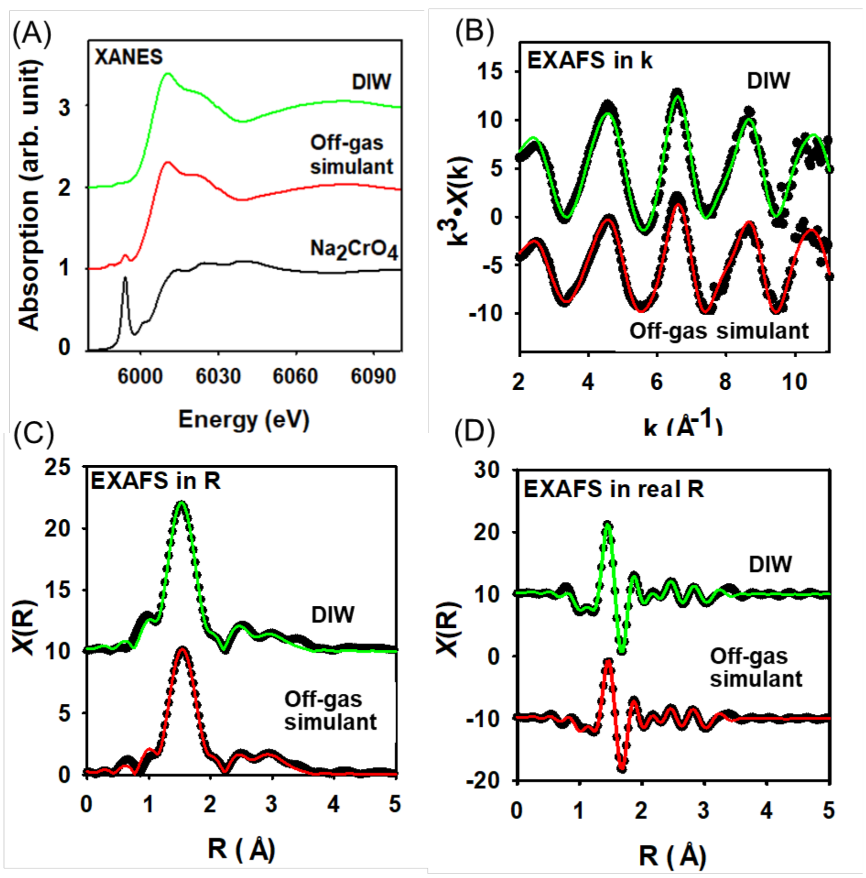

Figure 5: Cr K-edge XANES and EXAFS spectra of two LDH─Mo_3S_{13} samples after Cr treatments in DIW and off-gas simulant, XANES, together with the spectrum of Na_2CrO_4 (A), EXAFS data in k space (B), EXAFS data in R space (C), and EXAFS data in real R space (D). Dotted and solid-colored lines in EXAFS represent experimental and fitted data, respectively.

XPS and XANES predominantly show the removal of chromium involves reduction of Cr^{6+} to Cr^{3+}. The CrO_4^{2-} anion adopts a tetrahedral geometry while the Cr^{3+} species remains predominantly in an octahedrally coordinated environment. This change in coordination number and the geometry are further demonstrated by Cr K-edge EXAFS data (Figures 5B-D). The fitted EXAFS parameters of these samples are summarized in Table 1, in comparison with X-ray diffraction data of Cr_2O_3.[46] The Cr K-edge EXAFS data of the sorbent sample exposed to CrO_4^{2-} in DIW was fitted with octahedral Cr-O paths at a Cr-O distance of 1.971 ± 0.005 Å with a fitted coordination number of 5.10 ± 0.39, and three Cr-Cr paths at 2.54 ± 0.03, 3.09 ± 0.03. and 3.38 ± 0.03 Å, respectively, with the corresponding fixed coordination numbers obtained from Cr_2O_3 X-ray diffraction data.[46] The Cr-O octahedron in Cr_2O_3 displays three Cr-O bonds at a distance of 1.964 Å and three Cr-O bonds at a distance of 2.013 Å, but the EXAFS data fitting was kept with the same Cr-O bond distance to limit the fitting parameters. The fitted Cr-O bond distance of 1.971 Å and coordination number of 5.1 are comparable to those in Cr_2O_3, but the fitted bond distances for two of three Cr-Cr paths show larger variation compared to those in Cr_2O_3. However, the overall EXAFS data fitting of this sample was acceptable as measured by the R factor of 0.0026 (Table 1). Thus, the Cr K-edge EXAFS spectra of the sorbent exposed to CrO_4^{2-} in DIW confirmed that the Cr species associated with the sorbent was likely Cr_2O_3 or $Cr(OH)_3$.

The Cr K-edge EXAFS data of the sorbent sample exposed to CrO_4^{2-} in off-gas simulant was also fitted using Cr_2O_3 structure model. Although its Cr K-edge XANES indicated that 15.4% of Cr was CrO_4^{2-}, the EXAFS data fitting did not permit more parameters with the addition of another phase. In general, the fitted EAXFS parameters for the sorbent exposed to CrO_4^{2-} in the off-gas simulant were similar to those of the sorbent exposed to CrO_4^{2-} in DIW (Table 1) and the overall fitting of this sample was acceptable as measured by the R factor of 0.0039 (Table 1).

However, the fitted Cr-O coordination number for this sample was 3.72 ± 0.35 (Table 1), which was significantly smaller than the Cr-O coordination number of 5.1 in the sample retrieved from DIW and the Cr-O coordination number of 6 in Cr_2O_3. Except for the common error of up to 20% for fitted coordination number from EXAFS data fitting, this discrepancy might also indicate that a small portion of Cr in this sample was tetrahedral CrO_4^{2-}. Thus, the Cr K-edge EXAFS spectra of the sorbent exposed to CrO_4^{2-} in off-gas simulant confirmed that the dominant Cr species associated with the sorbent was likely Cr_2O_3 or $Cr(OH)_3$, but a small amount of CrO_4^{2-} was also present, consistent with its Cr K-edge XANES data discussed above.

Table 1: Cr K-edge fitting data for Cr species after interactions of LDH─Mo_3S_{13} with CrO_4^{2-} in water and in the simulated LAW off-gas condensate.

Samples	Path	Bond distance (Å)	Coordination number	Debye–Waller factor, σ2 (Å2)	ΔE0 (eV)	R-factor
DIW	Cr-O2	1.971±0.005	5.10±0.39	0.0026±0.0007	3.2±0.8	0.0026
	Cr-Cr1	2.54±0.03	1	0.0149±0.0047		
	Cr-Cr2	3.09±0.03	3	0.0155±0.0039		
	Cr-Cr3	3.38±0.03	3	0.0111±0.0027		
Off-gas simulant	Cr-O2	1.976±0.005	3.72±0.35	0.0011±0.0009	3.7±1.0	0.0039
	Cr-Cr1	2.56±0.05	1	0.0185±0.0072		
	Cr-Cr2	3.09±0.05	3	0.0216±0.0072		
	Cr-Cr3	3.39±0.02	3	0.0108±0.0025		
Cr_2O_3	Cr-O1	1.964	3			
	Cr-O2	2.013	3			
	Cr-Cr1	2.650	1			
	Cr-Cr2	2.888	3			
	Cr-Cr3	3.425	3			

Mo L3-edge XANES reveals the presence of the dipole allowed 2p → 4d transition of Mo^{4+} at 2523.8 eV, indicating that Mo predominantly remains as Mo^{4+} in the post reacted solids, in agreement with XPS results (Figure S5).[65] The XANES of S K-edge shows peaks at about 2471.4, 2471.6 and 2471.7 eV for the pristine, water, and simulant treated samples, respectively. These peaks demonstrate the presence of sulfide species. The peak at 2481.9 eV can be ascribed to S^{6+} oxidation states which suggests concomitant oxidation of some of the sulfide groups of LDH─Mo_3S_{13}. Importantly, the intensity of the S^{6+} peaks sharply increase from the pristine to simulant treated LDH─Mo_3S_{13}, indicating a higher propensity of sulfide oxidation in the simulated solutions which further supports the reductive precipitation of Cr^{6+} to Cr^{3+}.

Altogether, an insight of the sorption mechanisms demonstrates that reductive precipitation is the dominant mechanism for the removal of TcO_4^-/CrO_4^{2-}, nevertheless, a small contribution of ion-exchange and/or surface adsorption cannot be ruled out, especially for the simulated off-gas condensate of the LAW melter. The reductive precipitation mechanism requires the use of S^{n-} (n = 1,2) and Mo^{4+} of the LDH-Mo_3S_{13} as the reductants to precipitate out the Cr^{3+} species. Overall, this study reveals that LDH─Mo_3S_{13} is a high performing sorbent of TcO_4^-/CrO_4^{2-} from defense nuclear legacy waste. We believe this finding advances our knowledge and points to design principles of materials that can accomplish excellent efficiency in complex high ionic strength solutions for the sequestration of pertechnetate and chromate anions from aqueous solutions.

ACKNOWLEDGEMENT

This work was partially supported by the US Department of Energy Minority Serving Institution Partnership Program (MSIPP) managed by the Savannah River National Laboratory under SRNS contract (RFP No. 0000542525 and 0000458357). SCR is thankful to the NSF Division of Chemistry (NSF-2100797). All the ICP-MS analysis were conducted at JSU's core research centers supported by RCMI (NIH grant: 1U54MD015929). X-ray Absorption Spectroscopy was performed at the SXRMB beamline of the Canadian Light Source, a national research facility of the University of Saskatchewan, which is supported by the Canada Foundation for Innovation

(CFI), the Natural Sciences and Engineering Research Council (NSERC), the National Research Council (NRC), the Canadian Institutes of Health Research (CIHR), the Government of Saskatchewan, and the University of Saskatchewan. Any use of trade, firm, or product names is for descriptive purposes only and does not imply endorsement by the U.S. Government. This work made use of the Keck-II facility of Northwestern University's NUANCE Center, which has received support from the SHyNE Resource (NSF ECCS-2025633), the IIN, and Northwestern's MRSEC program (NSF DMR-1720139).

Supplementary data Supplementary data contain details on uptake study as well as the characterization of the pristine and post adsorption LDH-Mo_3S_{13} which are found online at http:

AUTHOR CONTRIBUTIONS

This manuscript was written through the contributions of all authors. All authors have given approval to the final version of the manuscript.

Corresponding author

Dr. Saiful M. Islam

Email: muhammad.s.islam@jsums.edu

ORCHID ID: orcid.org/0000-0001-8518-1856

References

(1) Taylor-Pashow, K. M. L.; Poirier, M.; McCabe, D. J. *Bench Scale Experiments for the Remediation of Hanford Waste Treatment Plant Low Activity Waste Melter Off-Gas Condensate*; SRNL-STI-2017-00322; Savannah River Site (SRS), Aiken, SC (United States), **2017**. https://doi.org/10.2172/1377029.

(2) Wilmarth, W. R.; Lumetta, G. J.; Johnson, M. E.; Poirier, M. R.; Thompson, M. C.; Suggs, P. C.; Machara, N. P. Review: Waste-Pretreatment Technologies for Remediation of Legacy Defense Nuclear Wastes. *Solvent Extr. and Ion Exch.* **2011**, *29* (1), 1–48. https://doi.org/10.1080/07366299.2011.539134.

(3) Adamson, D. J.; Nash, C. A.; McCabe, D. J.; Crawford, C. L.; Wilmarth, W. R. *Laboratory Evaporation Testing Of Hanford Waste Treatment Plant Low Activity Waste Off-Gas Condensate Simulant*; SRNL-STI--2013-00713, 1117838; **2014**; p SRNL-STI--2013-00713, 1117838. https://doi.org/10.2172/1117838.

(4) Taylor-Pashow, K. M.; Nash, C. A.; Crawford, C. L.; McCabe, D. J.; Wilmarth, W. R. *Laboratory Scoping Tests Of Decontamination Of Hanford Waste Treatment Plant Low Activity Waste Off-Gas Condensate Simulant*; SRNL-STI-2013-00719; Savannah River Site (SRS), Aiken, SC (United States), **2014**. https://doi.org/10.2172/1116991.

(5) McCloy, J. S.; Riley, B. J.; Goel, A.; Liezers, M.; Schweiger, M. J.; Rodriguez, C. P.; Hrma, P.; Kim, D.-S.; Lukens, W. W.; Kruger, A. A. Rhenium Solubility in Borosilicate Nuclear Waste Glass: Implications for the Processing and Immobilization of Technetium-99. *Environ. Sci. Technol.* **2012**, *46* (22), 12616–12622. https://doi.org/10.1021/es302734y.

(6) Neeway, J. J.; Asmussen, R. M.; Lawter, A. R.; Bowden, M. E.; Lukens, W. W.; Sarma, D.; Riley, B. J.; Kanatzidis, M. G.; Qafoku, N. P. Removal of TcO_4^- from Representative Nuclear Waste Streams with Layered Potassium Metal Sulfide Materials. *Chem. Mater.* **2016**, *28* (11), 3976–3983. https://doi.org/10.1021/acs.chemmater.6b01296.

(7) Pearce, C. I.; Moore, R. C.; Morad, J. W.; Asmussen, R. M.; Chatterjee, S.; Lawter, A. R.; Levitskaia, T. G.; Neeway, J. J.; Qafoku, N. P.; Rigali, M. J.; Saslow, S. A.; Szecsody, J. E.; Thallapally, P. K.; Wang, G.; Freedman, V. L. Technetium Immobilization by Materials through Sorption and Redox-Driven Processes: A Literature Review. *Sci. Total Environ.* **2020**, *716*, 132849. https://doi.org/10.1016/j.scitotenv.2019.06.195.

(8) Banerjee, D.; Kim, D.; Schweiger, M. J.; Kruger, A. A.; Thallapally, P. K. Removal of TcO_4^- Ions from Solution: Materials and Future Outlook. *Chem. Soc. Rev.* **2016**, *45* (10), 2724–2739. https://doi.org/10.1039/C5CS00330J.

(9) Taylor-Pashow, K. M. L.; McCabe, D. J.; Nash, C. A. Tc Removal from the Waste Treatment and Immobilization Plant Low-Activity Waste Vitrification off-Gas Recycle. *Sep. Sci. Technol.* **2018**, *53* (12), 1925–1934. https://doi.org/10.1080/01496395.2017.1302952.

(10) Sheng, D.; Zhu, L.; Xu, C.; Xiao, C.; Wang, Y.; Wang, Y.; Chen, L.; Diwu, J.; Chen, J.; Chai, Z.; Albrecht-Schmitt, T.; Wang, S. Efficient and Selective Uptake of TcO_4^- by a Cationic Metal-Organic Framework Material with Open Ag+ Sites. *Environ. Sci. Technol.* **2017**. https://doi.org/10.1021/acs.est.7b00339.

(11) Pierce, E. M.; Mattigod, S. V.; Westsik, J. H.; Serne, R. J.; Icenhower, J. P.; Scheele, R. D.; Um, W.; Qafoku, N. *Review of Potential Candidate Stabilization Technologies for Liquid and Solid Secondary Waste Streams*; PNNL-19122; Pacific Northwest National Lab. (PNNL), Richland, WA (United States). Environmental Molecular Sciences Lab. (EMSL), 2010. https://doi.org/10.2172/978974.

(12) Hrma, P. R. *Retention of Halogens in Waste Glass*; PNNL-19361, 981571; 2010; p PNNL-19361, 981571. https://doi.org/10.2172/981571.

(13) Goel, A.; McCloy, J. S.; Pokorny, R.; Kruger, A. A. Challenges with Vitrification of Hanford High-Level Waste (HLW) to Borosilicate Glass – An Overview. *J. Non Cryst. Solids*: X**2019**, *4*, 100033. https://doi.org/10.1016/j.nocx.2019.100033.

(14) Johnson, F.; Stone, M.; McCabe, D. *Evaluation of Immobilizing Secondary Waste from a Proposed Treatment Process for Hanford WTP LAW Melter Condensate*; Savannah River Site (SRS), Aiken, SC (United States), **2018**.

(15) Pearce, C. I.; Moore, R. C.; Morad, J. W.; Asmussen, R. M.; Chatterjee, S.; Lawter, A. R.; Levitskaia, T. G.; Neeway, J. J.; Qafoku, N. P.; Rigali, M. J.; Saslow, S. A.; Szecsody, J. E.; Thallapally, P. K.; Wang, G.; Freedman, V. L. Technetium Immobilization by Materials through Sorption and Redox-Driven Processes: A Literature Review. *Sci. Total Environ.* **2020**, *716*, 132849. https://doi.org/10.1016/j.scitotenv.2019.06.195.

(16) Pearce, C. I.; Cordova, E. A.; Garcia, W. L.; Saslow, S. A.; Cantrell, K. J.; Morad, J. W.; Qafoku, O.; Matyáš, J.; Plymale, A. E.; Chatterjee, S.; Kang, J.; Colon, F. C.; Levitskaia, T. G.; Rigali, M. J.; Szecsody, J. E.; Heald, S. M.; Balasubramanian, M.; Wang, S.; Sun, D. T.; Queen, W. L.; Bontchev, R.; Moore, R. C.; Freedman, V. L. Evaluation of Materials for Iodine and Technetium Immobilization through Sorption and Redox-Driven Processes. *Sci. Total Environ.t* **2020**, *716*, 136167. https://doi.org/10.1016/j.scitotenv.2019.136167.

(17) Wharton, M. J.; Atkins, B.; Charnock, J. M.; Livens, F. R.; Pattrick, R. A. D.; Collison, D. An X-Ray Absorption Spectroscopy Study of the Coprecipitation of Tc and Re with Mackinawite (FeS). *Appl.Geochem.* **2000**, *15* (3), 347–354. https://doi.org/10.1016/S0883-2927(99)00045-1.

(18) Ma, L.; Islam, S. M.; Liu, H.; Zhao, J.; Sun, G.; Li, H.; Ma, S.; Kanatzidis, M. G. Selective and Efficient Removal of Toxic Oxoanions of As(III), As(V), and Cr(VI) by Layered Double Hydroxide Intercalated with MoS_4^{2-}. *Chem. Mater.* **2017**, *29* (7), 3274–3284. https://doi.org/10.1021/acs.chemmater.7b00618.

(19) Pan, J.; Liu, L.; Pan, H.; Yang, L.; Su, M.; Wei, C. A Feasibility Study of Metal Sulfide (FeS and MnS) on Simultaneous Denitrification and Chromate Reduction. *J. Hazard. Mater.* **2022**, *424*, 127491. https://doi.org/10.1016/j.jhazmat.2021.127491.

(20) Liu, H.; Yu, X. Hexavalent Chromium in Drinking Water: Chemistry, Challenges and Future Outlook on Sn(II)- and Photocatalyst-Based Treatment. *Front. Environ. Sci. Eng.* **2020**, *14* (5), 88. https://doi.org/10.1007/s11783-020-1267-4.

(21) Maset, E. R.; Sidhu, S. H.; Fisher, A.; Heydon, A.; Worsfold, P. J.; Cartwright, A. J.; Keith-Roach, M. J. Effect of Organic Co-Contaminants on Technetium and Rhenium Speciation and Solubility under

Reducing Conditions. *Environ. Sci. Technol.* **2006**, *40* (17), 5472–5477. https://doi.org/10.1021/es061157f.

(22) Kim, J.; Jung, P.-K.; Moon, H.-S.; Chon, C.-M. Reduction of Hexavalent Chromium by Pyrite-Rich Andesite in Different Anionic Solutions. *Env. Geol.* **2002**, *42* (6), 642–648. https://doi.org/10.1007/s00254-002-0567-2.

(23) Pearce, C. I.; Icenhower, J. P.; Asmussen, R. M.; Tratnyek, P. G.; Rosso, K. M.; Lukens, W. W.; Qafoku, N. P. Technetium Stabilization in Low-Solubility Sulfide Phases: A Review. *ACS Earth Space Chem.* **2018**, *2* (6), 532–547. https://doi.org/10.1021/acsearthspacechem.8b00015.

(24) Rathore, E.; Maji, K.; Biswas, K. Nature-Inspired Coral-like Layered $[Co_{0.79}Al_{0.21}(OH)_2(CO_3)_{0.11}]\cdot mH_2O$ for Fast Selective Ppb Level Capture of Cr(VI) from Contaminated Water. *Inorg. Chem.* **2021**, *60* (13), 10056–10063. https://doi.org/10.1021/acs.inorgchem.1c01479.

(25) Ginder-Vogel, M.; Borch, T.; Mayes, M. A.; Jardine, P. M.; Fendorf, S. Chromate Reduction and Retention Processes within Arid Subsurface Environments. *Environ. Sci. Technol.* **2005**, *39* (20), 7833–7839. https://doi.org/10.1021/es050535y.

(26) Yang, H.; Fei, H. Exfoliation of a Two-Dimensional Cationic Inorganic Network as a New Paradigm for High-Capacity CrVI-Anion Capture. *Chem. Commun.* **2017**, *53* (52), 7064–7067. https://doi.org/10.1039/C7CC04375A.

(27) Sylvester, P.; Rutherford, L. A.; Gonzalez-Martin, A.; Kim, J.; Rapko, B. M.; Lumetta, G. J. Ferrate Treatment for Removing Chromium from High-Level Radioactive Tank Waste. *Environ. Sci. Technol.* **2001**, *35* (1), 216–221. https://doi.org/10.1021/es001340n.

(28) Daily, W.; Ramirez, A.; Binley, A. Remote Monitoring of Leaks in Storage Tanks Using Electrical Resistance Tomography: Application at the Hanford Site. *JEEG* **2004**, *9* (1), 11–24. https://doi.org/10.4133/JEEG9.1.11.

(29) Routson, R. C.; Price, W. H.; Brown, D. J.; Fecht, K. R. *High-Level Waste Leakage from the 241-T-106 Tank at Hanford*(No. RHO-ST-14). Rockwell International Corp. Richland, WA (USA), **1979**.

(30) Zhao, H.; Deng, Y.; Harsh, J. B.; Flury, M.; Boyle, J. S. Alteration of Kaolinite to Cancrinite and Sodalite by Simulated Hanford Tank Waste and Its Impact on Cesium Retention. *Clays Clay Miner*.**2004**, *52* (1), 1–13. https://doi.org/10.1346/CCMN.2004.0520101.

(31) Samanta, P.; Chandra, P.; Dutta, S.; Desai, A. V.; Ghosh, S. K. Chemically Stable Ionic Viologen-Organic Network: An Efficient Scavenger of Toxic Oxo-Anions from Water. *Chem. Sci.* **2018**, *9* (40), 7874–7881. https://doi.org/10.1039/C8SC02456A.

(32) Fan, D.; Anitori, R. P.; Tebo, B. M.; Tratnyek, P. G.; Lezama Pacheco, J. S.; Kukkadapu, R. K.; Engelhard, M. H.; Bowden, M. E.; Kovarik, L.; Arey, B. W. Reductive Sequestration of Pertechnetate ($^{99}TcO_4^-$) by Nano Zerovalent Iron (NZVI) Transformed by Abiotic Sulfide. *Environ. Sci. Technol.* **2013**, *47* (10), 5302–5310. https://doi.org/10.1021/es304829z.

(33) Strickert, R.; Friedman, A. M.; Fried, S. The Sorption of Technetium and Iodine Radioisotopes by Various Minerals. *Nucl. Technol.* **1980**, *49* (2), 253–266. https://doi.org/10.13182/NT80-A32488.

(34) Huie, Z.; Jishu, Z.; Lanying, Z. Sorption of Radionuclides Technetium and Iodine on Minerals. *Radiochim. Acta* **1988**, *44–45* (1), 143–146. https://doi.org/10.1524/ract.1988.4445.1.143.

(35) Wang, Y.; Gao, H. Compositional and Structural Control on Anion Sorption Capability of Layered Double Hydroxides (LDHs). *J Colloid Interface Sci.* **2006**, *301* (1), 19–26. https://doi.org/10.1016/j.jcis.2006.04.061.

(36) Yang, L.; Xie, L.; Chu, M.; Wang, H.; Yuan, M.; Yu, Z.; Wang, C.; Yao, H.; Islam, S. M.; Shi, K.; Yan, D.; Ma, S.; Kanatzidis, M. G. $Mo_3S_{13}^{2-}$ Intercalated Layered Double Hydroxide: Highly Selective Removal of Heavy Metals and Simultaneous Reduction of Ag^+ Ions to Metallic Ag^0 Ribbons. *Angew. Chem.* **2021**, 134(1), e202112511 https://doi.org/10.1002/anie.202112511.

(37) Celik, A.; Baker, D. R.; Arslan, Z.; Zhu, X.; Blanton, A.; Nie, J.; Yang, S.; Ma, S.; Han, F. X.; Islam, S. M. Highly Efficient, Rapid, and Concurrent Removal of Toxic Heavy Metals by the Novel 2D Hybrid LDH–$[Sn_2S_6]$. *Chem. Eng. J.* **2021**, *426*, 131696. https://doi.org/10.1016/j.cej.2021.131696.

(38) Ma, S.; Fan, C.; Du, L.; Huang, G.; Yang, X.; Tang, W.; Makita, Y.; Ooi, K. Intercalation of Macrocyclic Crown Ether into Well-Crystallized LDH: Formation of Staging Structure and Secondary Host−Guest Reaction. *Chem. Mater.* **2009**, *21* (15), 3602–3610. https://doi.org/10.1021/cm9007393.

(39) Islam, S. M.; Cain, J. D.; Shi, F.; He, Y.; Peng, L.; Banerjee, A.; Subrahmanyam, K. S.; Li, Y.; Ma, S.; Dravid, V. P.; Grayson, M.; Kanatzidis, M. G. Conversion of Single Crystal $(NH_4)_2Mo_3S_{13}\cdot H_2O$ to Isomorphic Pseudocrystals of MoS_2 Nanoparticles. *Chem. Mater.* **2018**, *30* (11), 3847–3853. https://doi.org/10.1021/acs.chemmater.8b01247.

(40) Islam, S. M.; Sangwan, V. K.; Li, Y.; Kang, J.; Zhang, X.; He, Y.; Zhao, J.; Murthy, A.; Ma, S.; Dravid, V. P.; Hersam, M. C.; Kanatzidis, M. G. Abrupt Thermal Shock of $(NH_4)_2Mo_3S_{13}$ Leads to Ultrafast Synthesis of Porous Ensembles of MoS_2 Nanocrystals for High Gain Photodetectors. *ACS Appl. Mater. Interfaces* **2018**, *10* (44), 38193–38200. https://doi.org/10.1021/acsami.8b12406.

(41) Manos, M. J.; Ding, N.; Kanatzidis, M. G. Layered Metal Sulfides: Exceptionally Selective Agents for Radioactive Strontium Removal. *PNAS* **2008**, *105* (10), 3696–3699. https://doi.org/10.1073/pnas.0711528105.

(42) Freundlich, H. Über die Adsorption in Lösungen. *Zeitschrift für Physikalische Chemie* **1907**, *57U* (1), 385–470. https://doi.org/10.1515/zpch-1907-5723.

(43) Liu, T.; Yang, M.; Wang, T.; Yuan, Q. Prediction Strategy of Adsorption Equilibrium Time Based on Equilibrium and Kinetic Results To Isolate Taxifolin. *Ind. Eng. Chem. Res.* **2012**, *51* (1), 454–463. https://doi.org/10.1021/ie201197r.

(44) Langmuir, I. THE ADSORPTION OF GASES ON PLANE SURFACES OF GLASS, MICA AND PLATINUM. *J. Am. Chem. Soc.* **1918**, *40* (9), 1361–1403. https://doi.org/10.1021/ja02242a004.

(45) Ravel, B.; Newville, M. ATHENA, ARTEMIS, HEPHAESTUS: Data Analysis for X-Ray Absorption Spectroscopy Using IFEFFIT. *J. Synchrotron Radiat.* **2005**, *12* (Pt 4), 537–541. https://doi.org/10.1107/S0909049505012719.

(46) Sawada, H. Residual Electron Density Study of Chromium Sesquioxide by Crystal Structure and Scattering Factor Refinement. *Mater. Res. Bull.* **1994**, *29* (3), 239–245. https://doi.org/10.1016/0025-5408(94)90019-1.

(47) Ma, S.; Chen, Q.; Li, H.; Wang, P.; Islam, S. M.; Gu, Q.; Yang, X.; Kanatzidis, M. G. Highly Selective and Efficient Heavy Metal Capture with Polysulfide Intercalated Layered Double Hydroxides. *J. Mater. Chem. A* **2014**, *2* (26), 10280–10289. https://doi.org/10.1039/C4TA01203H.

(48) Ma, S.; Shim, Y.; Islam, S. M.; Subrahmanyam, K. S.; Wang, P.; Li, H.; Wang, S.; Yang, X.; Kanatzidis, M. G. Efficient Hg Vapor Capture with Polysulfide Intercalated Layered Double Hydroxides. *Chem. Mater.* **2014**, *26* (17), 5004–5011. https://doi.org/10.1021/cm5020477.

(49) US EPA, O. *Chromium in drinking water; US EPA: https://www.epa.gov/ sdwa/chromium-drinking-water.* https://19january2017snapshot.epa.gov/dwstandardsregulations/chromium-drinking-water (accessed 2021-12-12).

(50) World Health Organization. *Guidelines for Drinking-Water Quality: Second Addendum; WHO: 2008, Https://Www.Who.Int/Water_sanitation_health/Publications/ Gdwq3rev/En/.*, 3rd ed.; World Health Organization: Geneva, **2008**.

(51) Bai, P.; Dong, Z.; Wang, S.; Wang, X.; Li, Y.; Wang, Y.; Ma, Y.; Yan, W.; Zou, X.; Yu, J. A Layered Cationic Aluminum Oxyhydroxide as a Highly Efficient and Selective Trap for Heavy Metal Oxyanions. *Angew. Chem. Int. Ed.* **2020**, *59* (44), 19539–19544. https://doi.org/10.1002/anie.202005878.

(52) Rapti, S.; Pournara, A.; Sarma, D.; Papadas, I. T.; Armatas, G. S.; Tsipis, A. C.; Lazarides, T.; Kanatzidis, M. G.; Manos, M. J. Selective Capture of Hexavalent Chromium from an Anion-Exchange Column of Metal Organic Resin–Alginic Acid Composite. *Chem. Sci.* **2016**, *7* (3), 2427–2436. https://doi.org/10.1039/C5SC03732H.

(53) Vaddi, D. R.; Gurugubelli, T. R.; Koutavarapu, R.; Lee, D.-Y.; Shim, J. Bio-Stimulated Adsorption of Cr(VI) from Aqueous Solution by Groundnut Shell Activated Carbon@Al Embedded Material. *Catalysts* **2022**, *12* (3), 290. https://doi.org/10.3390/catal12030290.

(54) Manning, B. A.; Kiser, J. R.; Kwon, H.; Kanel, S. R. Spectroscopic Investigation of Cr(III)- and Cr(VI)-Treated Nanoscale Zerovalent Iron. *Environ. Sci. Technol.* **2007**, *41* (2), 586–592. https://doi.org/10.1021/es061721m.

(55) *Handbook of X-Ray Photoelectron Spectroscopy: A Reference Book of Standard Spectra for Identification and Interpretation of XPS Data*; Moulder, J. F., Stickle, W. F., Sobol, P. E., Bomben, K. D., Chastain, J., King Jr., R. C., Physical Electronics, Incorporation, Eds.; Physical Electronics: Eden Prairie, Minn., **1995**.

(56) Islam, S. M.; Im, J.; Freeman, A. J.; Kanatzidis, M. G. Ba_2HgS_5--a Molecular Trisulfide Salt with Dumbbell-like $(HgS_2)^{2-}$ Ions. *Inorg Chem* **2014**, *53* (9), 4698–4704. https://doi.org/10.1021/ic500388s.

(57) Ma, S.; Huang, L.; Ma, L.; Shim, Y.; Islam, S. M.; Wang, P.; Zhao, L.-D.; Wang, S.; Sun, G.; Yang, X.; Kanatzidis, M. G. Efficient Uranium Capture by Polysulfide/Layered Double Hydroxide Composites. *J. Am. Chem. Soc.* **2015**, *137* (10), 3670–3677. https://doi.org/10.1021/jacs.5b00762.

(58) Islam, S. M.; Vanishri, S.; Li, H.; Stoumpos, C. C.; Peters, John. A.; Sebastian, M.; Liu, Z.; Wang, S.; Haynes, A. S.; Im, J.; Freeman, A. J.; Wessels, B.; Kanatzidis, M. G. $Cs_2Hg_3S_4$: A Low-Dimensional Direct Bandgap Semiconductor. *Chem. Mater.* **2015**, *27* (1), 370–378. https://doi.org/10.1021/cm504089r.

(59) Yuan, M.; Yao, H.; Xie, L.; Liu, X.; Wang, H.; Islam, S. M.; Shi, K.; Yu, Z.; Sun, G.; Li, H.; Ma, S.; Kanatzidis, M. G. Polypyrrole–Mo_3S_{13}: An Efficient Sorbent for the Capture of Hg^{2+} and Highly Selective Extraction of Ag^+ over Cu^{2+}. *J. Am. Chem. Soc.* **2020**, *142* (3), 1574–1583. https://doi.org/10.1021/jacs.9b12196.

(60) Xie, L.; Yu, Z.; Islam, S. M.; Shi, K.; Cheng, Y.; Yuan, M.; Zhao, J.; Sun, G.; Li, H.; Ma, S.; Kanatzidis, M. G. Remarkable Acid Stability of Polypyrrole-MoS_4: A Highly Selective and Efficient Scavenger of Heavy Metals Over a Wide pH Range. *Adv. Funct. Mater.* **2018**, *28* (20), 1800502. https://doi.org/10.1002/adfm.201800502.

(61) Huang, W.; Jiao, J.; Ru, M.; Bai, Z.; Yuan, H.; Bao, Z.; Liang, Z. Localization and Speciation of Chromium in Coptis Chinensis Franch. Using Synchrotron Radiation X-Ray Technology and Laser Ablation ICP-MS. *Sci. Rep.* **2018**, *8* (1), 8603. https://doi.org/10.1038/s41598-018-26774-x.

(62) Werner, M.; Nico, P.; Guo, B.; Kennedy, I.; Anastasio, C. Laboratory Study of Simulated Atmospheric Transformations of Chromium in Ultrafine Combustion Aerosol Particles. *Aerosol Sci. Technol.* **2006**, *40* (7), 545–556. https://doi.org/10.1080/02786820600714353.

(63) Pinakidou, F.; Kaprara, E.; Katsikini, M.; Paloura, E. C.; Simeonidis, K.; Mitrakas, M. Sn(II) Oxy-Hydroxides as Potential Adsorbents for Cr(VI)-Uptake from Drinking Water: An X-Ray Absorption Study. *Sci. Total Environ.* **2016**, *551–552*, 246–253. https://doi.org/10.1016/j.scitotenv.2016.01.208.

(64) Farges, F. Chromium Speciation in Oxide-Type Compounds: Application to Minerals, Gems, Aqueous Solutions and Silicate Glasses. *Phys. Chem. Minerals* **2009**, *36* (8), 463–481. https://doi.org/10.1007/s00269-009-0293-3.

(65) George, S. J.; Drury, O. B.; Fu, J.; Friedrich, S.; Doonan, C. J.; George, G. N.; White, J. M.; Young, C. G.; Cramer, S. P. Molybdenum X-Ray Absorption Edges from 200 – 20,000 EV, The Benefits of Soft X-Ray Spectroscopy for Chemical Speciation. *J. Inorg. Biochem.* **2009**, *103* (2), 157–167. https://doi.org/10.1016/j.jinorgbio.2008.09.008.